

1 **Connecting surface emissions, convective uplifting, and long-range**  
2 **transport of carbon monoxide in the upper-troposphere: New**  
3 **observations from the Aura Microwave Limb Sounder**

4 Jonathan H. Jiang, Nathaniel J. Livesey, and Hui Su  
5 Jet Propulsion Laboratory, California Institute of Technology, Pasadena, California, U.S.A.

6 Lori Neary and John C. McConnell  
7 Department of Earth and Space Science and Engineering, York University, Toronto, Ontario, Canada

8 Nigel A. D. Richards,  
9 Institute for Atmospheric Science, School of Earth and Environment, University of Leeds, United Kingdom

10

11

12

13 Submitted Geophysical Research Letters

14

15 May 10, 2007

16

17

18

19

20

---

21 Jonathan H. Jiang, M/S 183-701, Jet Propulsion Laboratory, California Institute of Technology, 4800  
22 Oak Grove drive, Pasadena, California 91109-8099, U.S.A.

23 (Email: jonathan@mls.jpl.nasa.gov)

24

25

1 **Abstract**

2 Using 2 years of observations of carbon monoxide (CO) from the Microwave Limb Sounder  
3 (MLS) on the Aura satellite, we show that spatial distribution, temporal variation and long-range  
4 transport of CO in the upper troposphere are closely related to the surface emissions, deep-  
5 convection and horizontal winds. The upper tropospheric transport of CO from Southeast Asia  
6 across the Pacific to North America occurs most frequently during the northern summer when deep  
7 convection associated the Asian monsoon is clustered over the strong anthropogenic emission  
8 region.

9

10

11

12

13

14

15

16

17

18

19

20

21

22

23

24

## 1 **1. Introduction**

2 Human activities – industrial, agricultural and residential – cause vast quantities of natural and  
3 synthetic chemicals to be emitted into the atmosphere. One of these chemicals is carbon monoxide  
4 (CO), which is mostly formed by incomplete combustion of fossil and bio-fuels, and by bio-mass  
5 burning. The quasi-exponential growth in world population and industrialization over the past  
6 decades has led to a rapid growth in fossil fuel and bio-fuel emissions. In developing countries  
7 such as China and India, the industrial and residential sectors, consisting of the combustion of coal,  
8 kerosene, and bio-fuels in stoves, cookers, and heaters, as well as gasoline in automobiles,  
9 generate the majority of the local emissions [*Streets et al.* 2003]. The total global anthropogenic  
10 CO emission is estimated at ~655 Tg/year, of which about 47% is of Asian origin [*Bey et al.* 2001;  
11 *Yevich and Logan* 2003]. Global biomass-burning emits about 485 Tg/year of CO, of which Asia  
12 contributes nearly 30% [*Duncan et al.* 2003]. CO is also commonly used as a proxy of other  
13 pollutants, such as carbonaceous aerosols and black carbon. Although it is mostly emitted at the  
14 surface, CO can be rapidly uplifted into mid- and upper troposphere (UT) by convection, where it  
15 can be transported around the globe by the circulation. In addition to the emissions at surface, CO  
16 is also produced in the atmosphere through oxidation of methane and non-methane hydro-carbons  
17 by hydroxyl radical (OH). There are two major sinks of tropospheric CO: removal from the  
18 atmosphere through direct oxidation by OH and loss by transport to the stratosphere. The chemical  
19 lifetime of CO due to loss by OH varies between 2-8 months depending on latitude and season  
20 [*e.g., Schindell et al.* 2006]. The timescale for transport of CO into the lower stratosphere through  
21 upwelling advection in the tropics has been estimated to be several months [*Schoeberl et al.* 2006,  
22 *Liu et al.* 2007]. Its relatively long life time enables CO to be a good tracer of transport processes,  
23 such as the long-range transport of Asian pollutants across the Pacific.

1 A number of recent field observations have documented that chemical composition over the  
2 Western Pacific is frequently perturbed by the pollutant outflow from south Asia [e.g. *Huebert et*  
3 *al.* 2003; *Jacob et al.* 2003; *Kondo et al.* 2002]. There is also evidence from the surface and  
4 aircraft observations that shows the Asian pollution influences extend to North America [e.g.  
5 *Bertschi et al.* 2004; *Weiss-Penzias et al.* 2004; *Price et al.*, 2003, 2004; *Jaffe et al.* 2003;  
6 *Kotchenruther et al.* 2001], especially during spring and winter seasons. Many studies, however,  
7 are largely based on observations at lower, mid-troposphere or tropospheric column. Global  
8 observations that target at the UT are limited, where the distribution and variation of CO could be  
9 much different from the lower layers. Modeling analyses show that distribution, seasonal variation  
10 and transport of CO can vary significantly at different altitudes [e.g. *Liang et al.* 2003; *Stohl et al.*  
11 2002], but substantial differences exist between models in which the simulated UT CO exhibits  
12 different behaviors in seasonality [e.g. *Neary et al.* 2007].

13 The Microwave Limb Sounder (MLS) instrument [*Waters et al.* 2006] on the Aura satellite has  
14 been measuring upper tropospheric CO mixing ratios (in ppbv) since August 2004 [*Livesey et al.*  
15 2007]. Analysis of the MLS CO data has led to several important scientific discoveries including:  
16 trapping of polluted air over South Asia [*Li et al.* 2005]; a ‘short-circuit’ of CO and water vapor  
17 (H<sub>2</sub>O) transport path into the lower stratosphere [*Fu et al.* 2006]; a CO ‘tape recorder’ signal  
18 [*Schoeberl et al.* 2006] analogous to that first discovered in H<sub>2</sub>O [*Mote et al.* 1996]; and the  
19 influence of convection on UT composition [*Folkens et al.*, 2006]. The distribution and variations  
20 of UT CO are likely influenced by the seasonal variation and spatial patterns of surface emission  
21 sources, the seasonal movement of deep convection systems, and the seasonal change of  
22 tropospheric winds. The relative importance of these factors and how they connect together remain  
23 to be studied. From time to time episodic transport events are observed by MLS. Figure 1  
24 illustrates an example of one such transport event. The MLS observed CO averaged for 1-6 June

1 2006 at three UT pressure levels are shown, along with horizontal wind vectors at the same levels  
2 from the NCEP (National Centers for Environmental Prediction) analyses. The CO measurements  
3 are from the MLS version 1.5 dataset [Livesey *et al.* 2005], and have been screened to make sure  
4 they are not affected by clouds. The accuracy of the CO is estimated at ~30% or less for pressures  
5 147 hPa or less. At 215 hPa, there is a persistent factor of ~2 high bias, but the morphology is  
6 validated to be realistic [Livesey *et al.* 2007]. Two features in the CO distribution are clearly  
7 visible: the spatial patterns vary with height; and a CO plume extends from South Asia across the  
8 Pacific reaching the west coast of United States at 215 hPa. At 100 hPa, the enhanced CO is  
9 mostly concentrated over the Tibetan Plateau due to a strong “trapping effect” of the Asian  
10 summer monsoon anti-cyclone [Li *et al.* 2005]; At 147 hPa, the CO enhancements extend eastward  
11 to the middle North Pacific; At 215 hPa, a clear outflow of CO rich air is observed to emanate  
12 from South Asia, following the mid-latitude westerly jet across the North Pacific and eventually  
13 penetrating the western United States. Such CO enhancements and long-range transport events are  
14 observed sporadically in the MLS observations. Quantifying the seasonal variation of these  
15 transport events is important in order to characterize the processes controlling UT CO  
16 concentrations, and variability.

17 In this paper, we address the above issues using two-year (2004-2006) MLS CO observations  
18 with a focus on the Southeast Asian and North Pacific regions. Using a CO emission climatology,  
19 MLS cloud ice water content (IWC, Version 1.5), as well as outgoing longwave radiation (OLR)  
20 and winds from the NCEP analyses, we estimate the impact of surface emission, convection and  
21 tropospheric winds on the distribution and variation of CO in the UT, while also highlighting the  
22 seasonal variability of long-range transport of Asian pollutants across North Pacific. Description  
23 and validation of MLS CO and IWC data can be found in Livesey *et al.* [2007] and Wu *et al.*  
24 [2007] and thus are not discussed here.

## 1 2. Surface Emissions

2 We first examine the surface emissions of CO: their spatial distribution, seasonal changes and  
3 how CO may disperse immediately after release. In Figure 2, the color shading in the bottom two  
4 panels (a) and (b) shows the surface fluxes of CO from biomass-burning and anthropogenic  
5 sources, respectively. The biomass-burning emissions (Figure 2a) are from the climatological  
6 inventory described in *Duncan et al.* [2003]. Biomass burning has a strong seasonal variation,  
7 which oscillates from the northern to the southern sub-tropics over the course of a year. From  
8 October to April when the tropical rain belt associated with the Intertropical Convergence Zone  
9 (ITCZ) lies mostly in the southern hemisphere, the northern sub-tropics are under the influence of  
10 the descending branch of the Hadley cell and experience mostly dry conditions. Hence, forest fires  
11 frequently occur over the South Asia landmass, especially during second half of this “dry” period  
12 (in winter and spring). From May to September, the ITCZ lies in the northern hemisphere and is  
13 accompanied by active monsoonal rainfall, which suppresses biomass burning during this “wet”  
14 period. The anthropogenic emissions shown are from climatology inventory described in *Bey et*  
15 *al.* [2001] and *Yevich and Logan* [2003], which consists of mainly fossil fuel combustion (e.g.  
16 coal-fired power plants) and bio-fuels. These anthropogenic emissions are located at human  
17 population centers and are relatively stable with little seasonal variations (Figure 2b).

18 To illustrate how the CO-loaded air may be dispersed and transported after being released from  
19 the source region, sea-level-pressures (SLP) and near-surface (900 hPa) horizontal winds from  
20 NCEP analyses are over-plotted in Figure 2 (a) and (b), respectively. Low SLP indicates the  
21 regions of convergence and ascent, whereas high SLP shows region of divergence and subsidence.  
22 The near-surface winds give an indication of the direction in which the emitted CO could disperse  
23 in the boundary layer and lower troposphere. In January, strong north-westerlies would lead to  
24 transport of the Asian anthropogenic CO to North Pacific in the lower troposphere (see wind

1 contours in Figure 2b, Jan06), but it is unlikely to be lifted up to the UT because of the strong  
2 subsidence over Asia, indicated by the high SLP contours in Figure 2a (Jan06). In July, the  
3 westerly winds are the weakest compared to other seasons and are located further north between  
4 30°N and 50°N. There is also strong ascent associated with the Asian summer monsoon  
5 convection that can loft CO into the mid-troposphere and UT. Spring and fall seasons represent  
6 transition periods where the mid-latitude westerlies are stronger than those of summer but  
7 convection over Asia is modest. In April, eastward winds occur throughout latitudes between 10°N  
8 and 50°N with moderate ascending air at equatorial South Asia, favoring upward transport of  
9 Asian CO. In the fall, the eastward winds are located further north at latitudes poleward of 30°N,  
10 far away from the tropical convection zone, a condition under which the vertical transport of CO  
11 may be limited.

### 12 **3. Deep Convection**

13 Deep convection is a process that can cause rapid injection of boundary layer CO into the UT.  
14 Figure 2 (c) shows the MLS observed IWC, over-plotted with NCEP 240 W/m<sup>2</sup> OLR contour.  
15 Regions with large MLS IWC are generally collocated with regions of low OLR, so that we can  
16 use IWC as a good indicator of deep-convection [Su *et al.* 2006]. The strength and location of deep  
17 convection (shown by large IWC) vary considerably from season to season. From winter to  
18 summer, the maximum of the tropical convection migrates northward from the Western Pacific  
19 (just south of the equator) to South and Southeast Asian. During summer, strong convection is  
20 associated with Asian summer monsoon (ASM) with the largest IWC at northern subtropics over  
21 the landmass of North India, South and Southeast China. The summer-time winds there are  
22 characterized by a strong convergence at the lower troposphere and a divergence in the UT. The  
23 latter is associated with the South Asian anticyclone (SAA), as a response to the elevated surface  
24 heating over the Tibetan Plateau and monsoonal diabatic heating. The associated monsoon

1 circulation and the SAA result in rapid vertical transport of polluted boundary layer air in this  
2 region. This convective pattern usually starts in late spring and lasts throughout the summer until  
3 the convective activity retreats southward to the ocean in mid-fall.

#### 4 **4. Upper Tropospheric CO**

5 Figure 2 (d), (e) and (f) show monthly means of MLS measured CO at 215, 147 and 100 hPa  
6 pressure levels over-plotted with the NCEP horizontal winds at the same height and during the  
7 same period. Clearly there is a high degree of seasonal variability in upper tropospheric CO. In  
8 January, even though there is biomass burning emission in Southern Asia, but convective activity  
9 is located further south in the maritime continent, and no significant amount of CO emissions are  
10 lifted into the UT over Southern Asia. In April, the convection pattern shifts northward, partially  
11 overlapping with the Southern Asia biomass burning region. However, the center of strong deep  
12 convection is still located further south, resulting in only moderate CO enhancement in the UT  
13 over Southern Asia. Outflow of CO from Southern Asia can be seen at 215 and 147 hPa pressure  
14 levels, indicating transport of upper tropospheric air into North Pacific. In July, heavy precipitation  
15 extinguishes most of the biomass burning in South Asia region. At same time, deep convection  
16 over land associated with the ASM carries large amount of anthropogenically polluted boundary  
17 layer air into the UT, resulting in high concentrations of CO over South Asia. The SAA is located  
18 over the Tibetan Plateau, with strong northeasterly winds on the southern flank of the Plateau. At  
19 147 to 100 hPa, elevated concentrations of CO are observed over India and across central and  
20 eastern China, where the upper level anticyclone prevails. Enhanced CO concentrations also  
21 extend from Southeast Asia to the Arabian Sea, transported by the strong easterly winds to the  
22 south of the SAA. The existence of SAA prevents rapid outflow of the accumulated CO over the  
23 region [*Randel and Park 2006*], a phenomena termed SAA “trapping effect”. The CO observations  
24 from MLS are broadly consistent with the large-scale wind patterns (Figure 2e and 2f, July 06). At

1 215 hPa (Figure 1d, July 06), the anti-cyclonic flow is weaker than that at upper levels. Substantial  
2 CO enhancement in the Pacific can be seen at this altitude, indicating long-range transport of CO  
3 rich air by westerly winds. Further north in Eurasia (~60°N, Fig. 1a), there is bio-mass burning but  
4 its influence on UT CO is limited due to the weak convection in that region. The amount of upper  
5 tropospheric CO in the fall season is lower than that in summer, but somewhat higher than those in  
6 spring and winter.

### 7 **5. Seasonality of Long-range Transport**

8 To first order, the seasonal variation of the Asian pollution outflow in the UT to North Pacific  
9 reflects mainly the seasonality of deep convection and mid-latitude winds as the large  
10 anthropogenic emissions do not vary much with season. But there are also impacts of the biomass  
11 burning in the tropics which varies with season.

12 Figure 3 shows the seasonal variation of UT CO and its connection with deep convection and  
13 surface emission sources. We consider three separate regions: Southeast Asia (SEA), which  
14 contains most of the emission sources; the Northwest Pacific (NWP), located downwind from the  
15 emission sources, offshore of China; and the Northeast Pacific (NEP), which is further down-  
16 stream close to the North America coast. The upper panels in Figure 3 illustrate the monthly mean  
17 quantities of MLS measured CO anomaly (thick green-line) and IWC (blue-line), both at 147 hPa,  
18 and NCEP OLR minus 240 W/m<sup>2</sup> (black-line). All quantities are normalized so that the maximum  
19 absolute value is 1. The CO anomaly refers to the departure of monthly mean CO from its 2-year  
20 mean. The lower panels are the monthly mean CO emissions from the biomass burning (dashed-  
21 line) and anthropogenic (solid-line) sources.

22 The seasonal variability in UT CO over the SEA closely follows the seasonal cycle of deep-  
23 convection indicated by OLR and IWC. The upper panel of Figure 3a shows that the CO over the  
24 Southeast Asia reaches the maximum in the mid-summer (July), when the convection is the

1 strongest. The biomass burning in SEA peaks in March but is smallest in summer and fall (see  
2 lower panel of Figure 3a). Therefore the maximum UT CO loading in summer months above the  
3 SE Asia is mostly from anthropogenic emissions, which are almost constant throughout the year.  
4 The scatter plots shown in Figure 4a further illustrate this convection influence on the 147 hPa CO  
5 loading. For the SEA region with abundant anthropogenic emission, there is a clear positive  
6 correlation between the observed CO and IWC, with a correlation coefficient of 0.6, statistically  
7 significant above the 95% level. This indicates a clear signal of convective transport of CO rich air  
8 in the UT.

9 In the NWP just off the east coast of China and Japan, there is little CO emission over the  
10 ocean surface, except from some scattered islands. Also there is smaller variation of convection in  
11 NWP compared to that in SEA, as indicated by the smaller changes in the OLR. Nevertheless, a  
12 weaker but still positive correlation exists between the CO and IWC (Figure 4b) at 147 hPa with  
13 correlation factor of 0.3, and the seasonal variation of CO occurs at the same phase as IWC - peaks  
14 in summer and dips in winter (Figure 3b). This may suggest that the outflow of CO rich air and the  
15 detrainment of cirrus clouds are from the same source region of SEA and are transported by  
16 westerly winds.

17 Over the NEP just west of the U.S. west coast, there is neither biomass burning nor  
18 anthropogenic emission sources. The variation of CO is not correlated with local convection as  
19 illustrated both by the time-series (Figure 3c) and by the scatter plots (Figure 4c). The correlation  
20 coefficient between the CO and IWC is less than 0.07. The seasonal variation of CO there is thus  
21 likely controlled by the long-range transport from SEA. It is also interesting to see that from NWP  
22 to NEP, the CO maximum becomes broader – it lasts longer into September, 2 months after peak  
23 CO in SEA. It usually takes a few days to a week for air to travel across the Pacific. The 2-month  
24 duration of the CO maximum is thus not the time scale for traveling across the Pacific but could

1 imply the residence lifetime of CO is about 2 months as the CO rich air meanders in the UT for  
2 about 2-month before it dissipates.

### 3 **6. Conclusion**

4 We have presented MLS UT CO observations in 2004-2006 with a focus on the Southeast Asia  
5 and the North Pacific region, and examined the connection of the observed UT CO pattern to  
6 surface emission and deep convection. The relationship between surface emission, deep-  
7 convection and long-range transport and their impact on the UT CO loadings, is summarized in  
8 Figure 5, in which the monthly mean MLS CO mixing ratios at 147 hPa gridded on the  
9  $8^\circ(\text{longitude}) \times 4^\circ(\text{latitude})$  grid-boxes in the northern hemisphere ( $0^\circ\text{-}90^\circ\text{N}$ ) from September  
10 2004 to September 2006 are binned according to the total (anthropogenic and biomass burning)  
11 CO surface emissions (x-axis) and the MLS IWC (y-axis). In general, the CO mixing ratio is high  
12 when convection is strong, indicated by the ascending arrow to the left of the y-axis. With the  
13 presence of deep convection, CO concentration roughly increases with increasing surface emission  
14 (see the arrow above the figure). When deep convection is absent, the UT CO is generally low and  
15 bears little connection with surface emissions. Thus the variation of the UT CO may result from  
16 long-range transport, as indicated by the dashed arrow near the x-axis. Interestingly, the 4 corners  
17 in Figure 5 represent four typical regimes of CO variability in the UT, each of which bears a  
18 distinct character of the relations among surface emission, deep convection, and horizontal  
19 transport of CO.

20 **Regime I:** Both surface emission and convection are strong; the maximum UT CO concentrations  
21 in this regime result from vigorous convective deposition of surface emission. SEA in summer is a  
22 typical Regime I, where strong deep convection is coupled with anthropogenic emission.

23 **Regime II:** There is strong convection but very little surface emission; the high CO in this regime  
24 may come from transport at the same height or convective lifting of lower level CO that

1 transported from other source regions. The NWP region shown in Figure 4b shows some  
2 characteristics of this regime. On daily basis, there are also regions with low CO concentration and  
3 zero surface emission but considerable convection, which are not shown in Figure 5 (Note the log-  
4 scale x-axis does not start at zero).

5 **Regime III:** There is no convection and no surface emission; the CO enhancements in this regime  
6 may indicate long-range transport of CO rich air from other regions at same altitude. The NE P  
7 shown in Figure 4c belongs to this category.

8 **Regime IV:** The surface emissions are strong but no convection is present so that a relatively small  
9 fraction of emissions make it to the 147 hPa level. The lack of CO enhancement in this regime  
10 means that horizontal transport of CO is also limited. For example, the Eurasia region in July 06  
11 (Figure 1a, Jul 06) experienced a strong bio-mass burning, but no CO enhancement (Figure 1e),  
12 due to lack of deep convection and horizontal transport.

13 Based on MLS CO observations, the highest CO concentrations in the northern hemisphere UT  
14 occur in summer when deep convection reaches peak intensity. At that time, the surface emission  
15 of CO is dominated by anthropogenic source. During winter and spring, the CO concentration in  
16 the UT is relatively weak despite of strong biomass-burning events, mainly due to the lack of deep  
17 convection directly over the emission source. The UT CO observed by MLS thus includes a clear  
18 fingerprint of Asian anthropogenic pollution in the global circulation and air quality.

## 19 **Acknowledgements**

20 This work was conducted at the Jet Propulsion Laboratory, California Institute of Technology  
21 supported by NASA. We thank Joe Waters, Michelle Santee, William Read, Dong Wu and all other  
22 colleagues in the MLS Science Team for support, as well as Qinbin Li and Chenxia Cai for useful  
23 discussions. LN and JCM wish to thank the Canadian Foundation for Climate and Atmospheric  
24 Science for support via MAQNet grant.

## 1 **References**

- 2 Bertschi, I.T., D.A. Jaffe, L. Jaegl, H.U. Price, J. B. Dennison (2004), PHOBEA/ITCT 2002 airborne  
3 observations of transpacific transport of ozone, CO, volatile organic compounds, and aerosols to  
4 the northeast Pacific: Impacts of Asian anthropogenic and Siberian boreal fire emissions, *J.*  
5 *Geophys. Res.*, 109, D23S12, doi:10.1029/2003JD004328.
- 6 Bey, I., D. J. Jacob, J. A. Logan, R. M. Yantosca (2001), Asian chemical outflow to the Pacific in  
7 spring: Origins, pathways, and budgets, *J. Geophys. Res.*, 106(D19), doi:10.1029/2001JD000806.
- 8 Duncan B.N., R.V. Martin, A.C. Staudt, R.Yevich, and J.A. Logan, Interannual and seasonal  
9 variability of biomass burning emissions constrained by satellite observations (2003), *J. Geophys.*  
10 *Res.*, 108 (D2), 4100, doi:10.1029/2002JD002378.
- 11 Folkins, I., et al., Seasonal cycles of O<sub>3</sub>, CO, and convective outflow at the tropical tropopause (2006),  
12 *Geophys. Res. Lett.* 33, L12802, doi:10.1029/2006GL02594.
- 13 Fu, R. et al., Short circuit of water vapor and polluted air to the global stratosphere by convective  
14 transport over the Tibetan Plateau (2006), *Proc. Nat. Acad. Sci.* 103, 5664-5669.
- 15 Huebert B.J., et al., An overview of ACE-Asia: Strategies for quantifying the relationships between  
16 Asian aerosols and their climatic impacts (2003), *J. Geophys. Res.*, 108(D23), doi:10.1029/  
17 2003JD003550.
- 18 Jacob D.J., et al., Transport and Chemical Evolution over the Pacific (TRACE-P) aircraft mission:  
19 Design, execution, and first results (2003), *J. Geophys. Res.*, 108(D20), doi:10.1029/  
20 2002JD003276.
- 21 Jaffe, D., et al., Transport of Asian air pollution to North America (1999), *Geophys. Res. Lett.*, 26(6),  
22 711-714, 10.1029/1999GL900100.
- 23 Jaffe D.A. et al., Comment on "Mercury concentrations in coastal California precipitation: Evidence of  
24 local and trans-Pacific fluxes of mercury to North America" by Steding and Flegal [2002] (2003).  
25 *J. Geophys. Res.* Vol. 108(D17), doi: 10.1029/2003JD003504.

1 Kondo Y. et al., Preface to Special Section on Biomass Burning and Lightning Experiment (BIBLE)  
2 (2002), *J. Geophys. Res.*, 107, doi: 10.1029/2002JD002401

3 Kondo Y., et al., Photochemistry of ozone over the western Pacific from winter to spring (2004), *J.*  
4 *Geophys. Res.*, 109, D23S02, doi:10.1029/2004JD 004871.

5 Kotchenruther, R. A. et al., Erratum: Observations of ozone and related species in the northeast Pacific  
6 during the PHOBEA campaigns, 2, Airborne observations (2001), *J. Geophys. Res.*, 106(D17),  
7 20507-20508, 10.1029/2001 JD000962.

8 Liang Q., L. Jaegl, D. A. Jaffe, P. Weiss-Penzias, and A. Heckman, J. A. Snow, Long-range transport  
9 of Asian pollution to the northeast Pacific: Seasonal variations and transport pathways of carbon  
10 monoxide (2004), *J. Geophys. Res.*, 109, D23S07, doi:10.1029/2003JD004402.

11 Neary, L., J. H. Jiang, J. C. McConnell, H. Su, and N. J. Livesey, Comparisons of Aura MLS CO  
12 measurements with GEM-AQ and GEOS-CHEM simulations, to be submitted, 2007.

13 Li, Q.B. et al., Convective outflow of South Asian pollution: A global CTM simulation compared with  
14 EOS MLS observations (2005), *Geophys. Res. Lett.* 32, L14826, doi:10.1029/2005GL022762.

15 Liu, C., E., Zipser, T., Garrett, J. H. Jiang, H. Su, How do the water vapor and carbon monoxide “tape  
16 recorder” start near the tropical tropopause? (2007), *Geophys. Res. Lett.*, 34, L09804, doi:10.1029/  
17 2006GL029234.

18 Livesey, N. J. et al., Validation of Aura Microwave Limb Sounder O3 and CO observations in the  
19 upper troposphere and lower stratosphere, *J. Geophys. Res.*, submitted, 2007.

20 Mote, P.W. et al., An atmospheric tape recorder: the imprint of tropical tropopause temperatures on  
21 stratospheric water vapor (1996), *J. Geophys. Res.* 101, 3989-4006.

22 Price H.U., D.A. Jaffe, P.V. Doskey, I. McKendry, and T.L. Anderson, Vertical profiles of O3,  
23 aerosols, CO and NMHCs in the Northeast Pacific during the TRACE-P and ACE-ASIA  
24 experiments (2003), *J. Geophys. Res.*, 108 (D20), doi:10.1029/ 2002JD002930.

1 Price H.U., D.A. Jaffe, O.R. Cooper, and P.V. Doskey (2004), Photo-chemistry, ozone production, and  
2 dilution during long-range transport episodes from Eurasia to the northwest United States, *J.*  
3 *Geophys. Res.*, 109, D23S13, doi:10.1029/2003JD004400.

4 Randel W.J. and M. Park, Deep convective influence on the Asian summer monsoon anticyclone and  
5 associated tracer variability observed with Atmospheric Infrared Sounder (AIRS) (2006), *J.*  
6 *Geophys. Res.*, 111, D12314, doi:10.1029/2005JD006490.

7 Schoeberl M.R. et al., The carbon monoxide tape recorder (2006), *Geophys. Res. Lett.*, 33, L12811,  
8 doi:10.1029/2006GL026178.

9 Shindell, D. T., et al., Multimodel simulations of carbon monoxide: Comparison with observations and  
10 projected near-future changes (2006), *J. Geophys. Res.*, 111, D19306, doi:10.1029/2006JD007100.

11 Stohl A. et al., On the pathways and timescales of intercontinental air pollution transport (2002), *J.*  
12 *Geophys. Res.*, 107 (D23), doi: 10.1029/2001JD001396.

13 Streets D. G., et al., An inventory of gaseous and primary aerosol emissions in Asia in the year 2000  
14 (2003), *J. Geophys. Res.*, 108 (D21), doi: 10.1029/2002JD003093.

15 Waters, J. W. et al., The Earth Observing System Microwave Limb Sounder (EOS MLS) on the Aura  
16 satellite (2006), *IEEE Trans. Geosci. Remote Sensing* 44, no. 5, 1075-1092.

17 Wu et al., Validation of the Aura MLS cloud ice water content (IWC) measurements (2007, *J.*  
18 *Geophys. Res.*, submitted.

19 Weiss-Penzias P., D. A. Jaffe, L. Jaegl, Q. Liang (2004), Influence of long-range-transported pollution  
20 on the annual and diurnal cycles of carbon monoxide and ozone at Cheeka Peak Observatory, *J.*  
21 *Geophys. Res.*, 109, D23S14, doi:10.1029/2004JD004505.

22 Yevich R., J. A. Logan, An assessment of biofuel use and burning of agricultural waste in the  
23 developing world (2003), *Global Biogeochem. Cycles*, 17 (4), 1095, doi: 10.1029/2002GB001952.

24

1  
2  
3  
4  
5  
6  
7  
8  
9  
10  
11  
12  
13  
14  
15  
16  
17  
18  
19  
20  
21  
22  
23  
24  
25

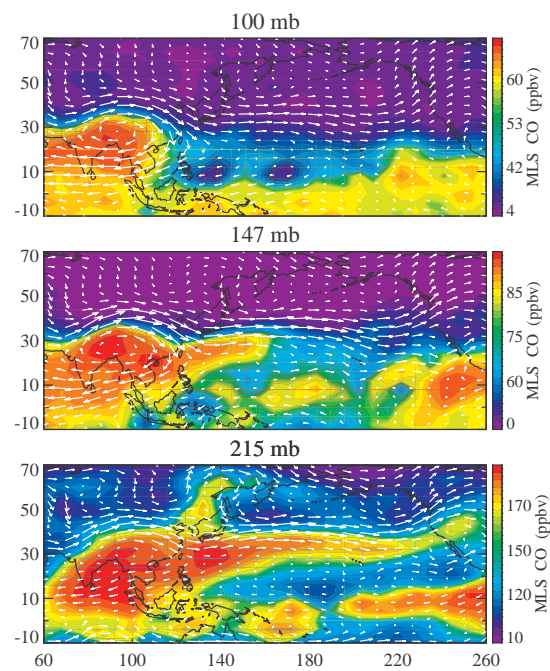
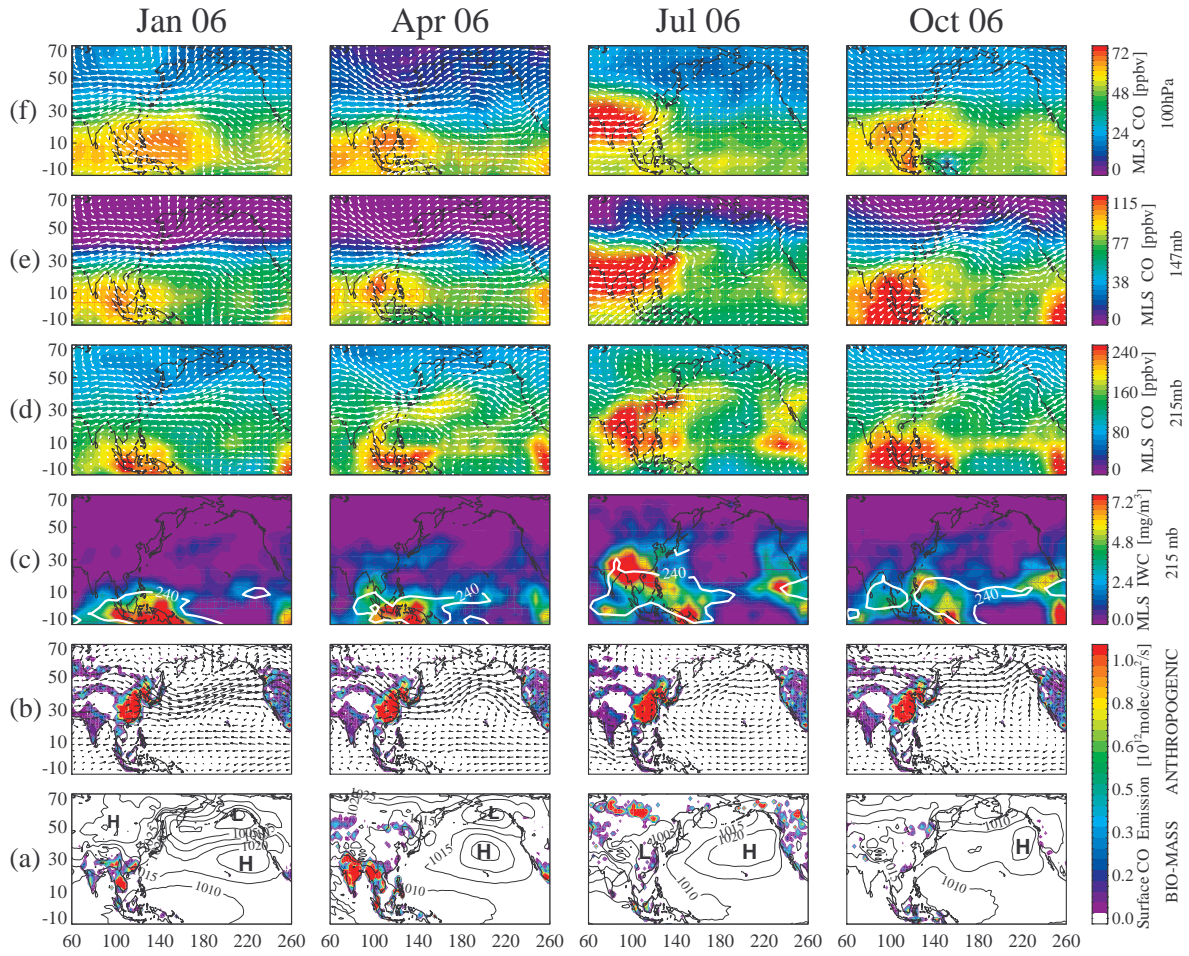


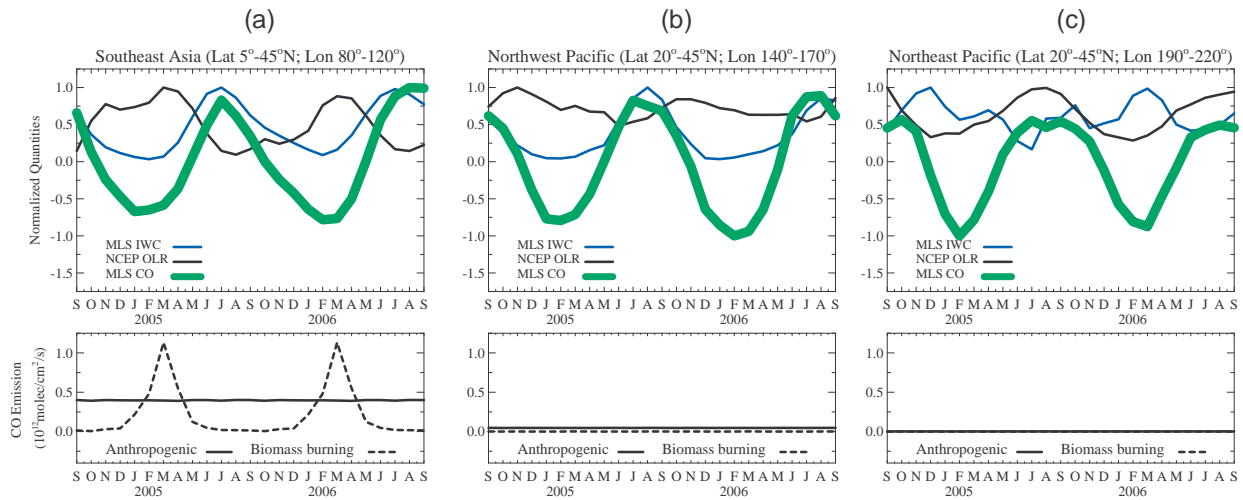
**Figure 1.** MLS measured CO mean mixing ratios for 1-6 June 2006 at three upper tropospheric pressure levels. The white arrows are the mean NCEP vector winds (U,V) at the same pressure levels. The data averaged on  $8^{\circ} \times 4^{\circ}$  longitude by latitude grids.



1

2 **Figure 2.** From left to right columns are monthly mean values (January, April, July, October  
 3 2006) averaged on  $8^{\circ} \times 4^{\circ}$  longitude by latitude grids. From bottom panel and up: (a) Bio-mass  
 4 burning emissions of CO (color-filled contour) and NCEP sea-level-pressesures (line-contour); (b)  
 5 Anthropogenic CO emissions (color-filled contour) and the 900 hPa vector winds (U+V) from  
 6 NCEP analysis; (c) MLS measured IWC at 215 hPa and the  $240 \text{ W/m}^2$  OLR contours in white line  
 7 contours for the tropical region from NCEP (low OLR in the high-latitude are not shown); (d), (e)  
 8 and (f) are MLS measured CO mixing ratios at 215hPa, 147hPa, and 100hPa pressure levels,  
 9 respectively, over plotted by NCEP vector winds at same pressures levels.

10



1

2 **Figure 3:** Top-panels: Time evolution of monthly mean 147 hPa MLS CO anomaly (thick green-  
 3 line), 147 hPa MLS IWC (blue-line), and NCEP OLR above 240 W/m<sup>2</sup> (black-line). Lower panels:  
 4 Time evolution of monthly mean CO emissions from biomass burning (dashed-line) and  
 5 anthropogenic (solid-line) sources. All data are normalized monthly mean quantities on 8° × 4°  
 6 longitude by latitude grids.

7

8

9

10

11

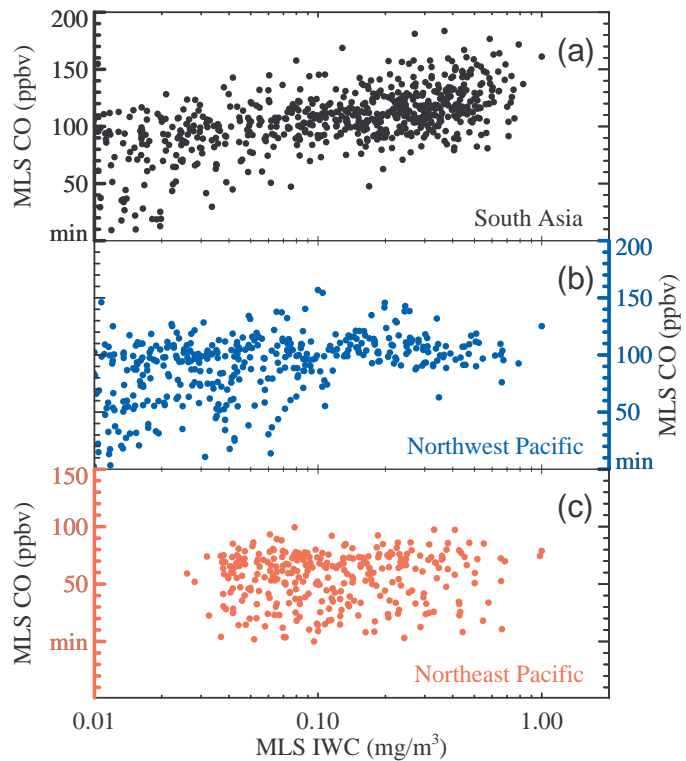
12

13

14

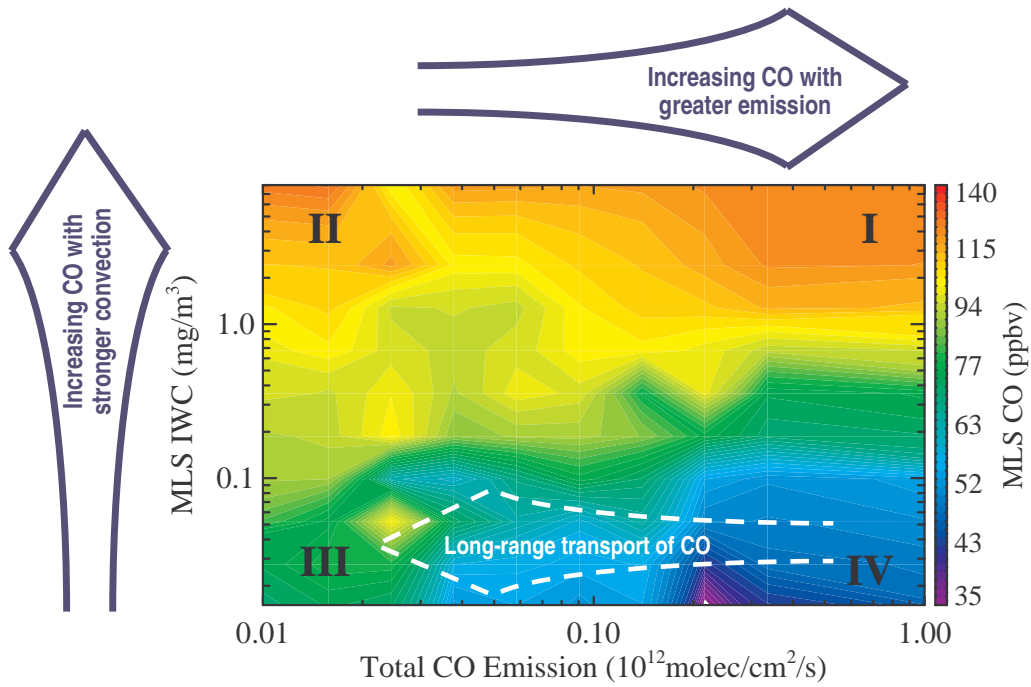
15

1  
2  
3  
4  
5  
6  
7  
8  
9  
10  
11  
12  
13  
14  
15  
16  
17  
18  
19  
20  
21  
22  
23  
24  
25  
26  
27  
28  
29



**Figure 4:** Scatter plots of MLS CO versus IWCs at 147 hPa for Southeast Asia (Lat: 5°-45°N; Lon: 80°-120°), Northwest Pacific (Lat: 20°-45°N; Lon: 140°-170°) and Northeast Pacific (Lat: 20°-45°N; Lon: 190°-220°). All data are from monthly means from September 2004 to September 2006 on 8° × 4° longitude by latitude grids.

1  
2



3 **Figure 5:** Contour plots of MLS CO mixing ratio at 147 hPa binned according to the total surface  
4 emission and MLS IWC amount at same pressure. All data are monthly mean values from  
5 September 2004 to September 2006 on  $8^\circ \times 4^\circ$  longitude by latitude grids.